7-2015

Conformations of Organophosphine Oxides

Nuwan De Silva
Iowa State University, ndesilva@iastate.edu

Federico Zahariev
Iowa State University, fzahari@iastate.edu

Benjamin P. Hay
Supramolecular Design Institute

Mark S. Gordon
Iowa State University, mgordon@iastate.edu

Theresa Lynn Windus
Iowa State University, twindus@iastate.edu

Conformations of Organophosphine Oxides

Abstract
The conformations of a series of organophosphine oxides, OP(CH3)2R, where R = methyl, ethyl, isopropyl, *tert*-butyl, vinyl, and phenyl, are predicted using the MP2/cc-pVTZ level of theory. Comparison of potential energy surfaces for rotation about P–C bonds with crystal structure data reveals a strong correlation between predicted location and energetics of minima and histograms of dihedral angle distributions observed in the solid state. In addition, the most stable conformers are those that minimize the extent of steric repulsion between adjacent rotor substituents, and the torsional barriers tend to increase with the steric bulk of the rotating alkyl group. MM3 force field parameters were adjusted to fit the MP2 results, providing a fast and accurate model for predicting organophosphine oxides shapes—an essential part of understanding the chemistry of these compounds. The predictive power of the modified MM3 model was tested against MP2/cc-pVTZ conformations for triethylphosphine oxide, OP(CH2CH3)3, and triphenylphosphine oxide, OP(Ph)3.

Disciplines
Chemistry

THE JOURNAL OF PHYSICAL CHEMISTRY A

Article

pubs.acs.org/JPCA

Conformations of Organophosphine Oxides

Nuwan De Silva,[†] Federico Zahariev,[†] Benjamin P. Hay,[‡] Mark S. Gordon,[†] and Theresa L. Windus*[,†]

[†]Ames Laboratory and Department of Chemistry, Iowa State University, Ames, Iowa 50011, United States

[‡]Supramolecular Design Institute, Oak Ridge, Tennessee 37830, United States

Supporting Information

ABSTRACT: The conformations of a series of organophosphine oxides, $OP(CH_3)_2R$, where R = methyl, ethyl, isopropyl, *tert*-butyl, vinyl, and phenyl, are predicted using the MP2/cc-pVTZ level of theory. Comparison of potential energy surfaces for rotation about P−C bonds with crystal structure data reveals a strong correlation between predicted location and energetics of minima and histograms of dihedral angle distributions observed in the solid state. In addition, the most stable conformers are those that minimize the extent of steric repulsion between adjacent rotor substituents, and the torsional barriers tend to increase with the steric bulk of the rotating alkyl group. MM3 force field parameters were adjusted to fit the MP2 results, providing a fast and accurate model for predicting organophosphine oxides shapes—an essential part of understanding the chemistry of these compounds. The predictive power of the modified MM3 model was tested against MP2/cc-pVTZ conformations for triethylphosphine oxide, $OP(CH_2CH_3)_3$, and triphenylphosphine oxide, $OP(Ph)_3$.

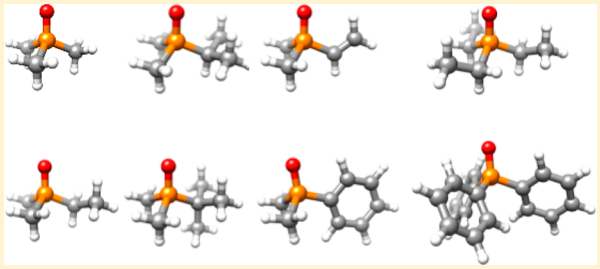

INTRODUCTION

Organophosphine oxides are compounds of the form OPR_3 where R = alkyl or aryl.[1] At a fundamental level, the nature of the PO bond in phosphine oxides is open to question[2−4] and can be represented by a combination of single- and triple-bond resonance structures or as a highly ionic dative P^+-O^- bond instead of the traditional double bond shown in most of the literature. The most recent estimate of the PO bond order in phosphine oxide is ∼1.5.[5] Nonetheless, for simplicity, this work follows the normal convention of using the P═O notation for the bond with the understanding that the PO bond is more complex in nature. Exhibiting a strong PO dipole moment, these compounds readily form complexes with metal ions and hydrogen bond donors.

Lipophilic analogues have long been studied as solvent extraction agents for rare earths, lanthanides, and actinides[6−12] and for protic organic species such as alcohols and carboxylic acids.[13,14] A well-known example, trioctylphosphine oxide (TOPO), has been used commercially in the recovery of uranium from wet process phosphoric acid[15] and recovery of byproduct acetic acid and furfural generated during sulfite wood pulping.[16] Development of novel metal chelating agents containing the phosphine oxide functional group remains an active area of research.[17−21] In addition to their utility as metal ion complexants, organophosphine oxides have application as Lewis base catalysts,[22−24] antitumor agents,[25] and electron transport materials in light-emitting diodes.[26−28]

The ability to predict the shapes of organophosphine oxides is essential for understanding the chemistry of these compounds. Quantum-mechanical (QM) calculations that include electron correlation, such as second-order Møller−Plesset perturbation theory (MP2),[29] can provide accurate information. However, correlated QM methods are computationally demanding. Even the most efficient wave function method that includes electronic correlation, MP2, scales as $\sim N^5$ in computer time, where N is related to the size of the chemical system. As a result, the use of correlated methods rapidly becomes intractable when applied to larger molecules or large numbers of smaller molecules. The latter situation frequently arises in conformational analysis where it may be necessary to perform thousands of geometry optimizations to locate all stable configurations of a molecule[30] and in structure-based computer-aided design applications involving the evaluation of thousands of candidates.[31−34] Given their computational efficiency, allowing full geometry optimizations in seconds, classical molecular mechanics (MM) models are the best choice for such applications.

If adequately parametrized, MM models are capable of yielding geometries and relative energies with an accuracy that rivals QM methods. The Allinger MM3 force field,[35] one of the most accurate MM models for small organic molecules,[36] was extended in 1998 to treat a subset of P(V) species, including phosphine oxides.[37,38] However, the extended parameter set was limited to aliphatic substituents, and the performance of the model with respect to organophosphine oxides was reported for only two examples, trimethylphosphine oxide and 1-methylphosphinane 1-oxide. Both the lack of parameters for unsaturated hydrocarbon substituents, such as vinyl and phenyl, and the desire to further benchmark this model against

Received: May 16, 2015
Revised: July 16, 2015
Published: July 17, 2015

DOI: 10.1021/acs.jpca.5b04687
J. Phys. Chem. A 2015, 119, 8765−8773

accurate QM methods provided motivation for the current study.

Herein we report conformational analyses and relative energetics for trimethylphosphine oxide, **1**, ethyl(dimethyl)-phosphine oxide, **2**, isopropyl(dimethyl)phosphine oxide, **3**, *tert*-butyl(dimethyl)phosphine oxide, **4**, vinyl(dimethyl)-phosphine oxide, **5**, phenyl(dimethyl)phosphine oxide, **6**, triethylphosphine oxide, **7**, and triphenylphosphine oxide, **8**. All possible minima generated by rotation about P−C bonds were evaluated at the MP2/cc-pVTZ level of theory. The results, which elucidate the preferred conformations of these species, were used to benchmark and improve the performance of the MM3 model.

Scheme 1

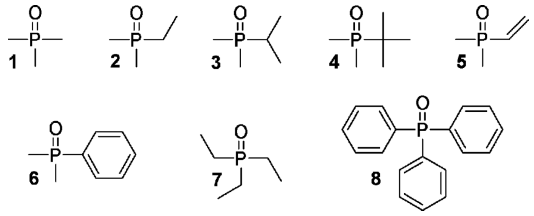

THEORETICAL METHODS

Electronic Structure Calculations. Calculations were performed with the GAMESS code[39,40] using second-order Møller−Plesset perturbation theory.[29] Calculations were done using the cc-pVTZ basis set,[41] including all valence electrons (frozen core) in the correlation treatment. Potential energy surfaces (PESs) for rotation about the P−C bonds in **1**−**8** were calculated by constraining one O═P−C−X (X = H or C) dihedral angle in the phosphine oxide and fully optimizing the remaining geometric degrees of freedom ($3N - 7$ internal degrees of freedom, where N is the number of atoms) with no symmetry constraints (C_1 symmetry). In each case the constrained optimizations were performed to obtain data from 0° to 360° at 5° increments. All geometry optimizations were converged to a very tight optimization convergence criterion, with the gradient being less than 0.00001 hartree/bohr.

Approximate positions of minima and transition states on the PESs were located by the above constrained optimization scheme. After removing the torsional constraints, MP2/cc-pVTZ calculations ($3N - 6$ internal degrees of freedom) yielded fully optimized geometries for the minima and transition states (absolute energies and atomic coordinates for these structures are provided as Supporting Information). Hessians were calculated and diagonalized at the optimized geometries of the minima and transition states at the MP2/cc-pVTZ level. Frequencies were used to characterize each stationary point as a minimum (no negative eigenvalues) or a transition state (one negative eigenvalue). The zero-point energy (ZPE) was obtained using the (real) harmonic frequencies. The zero-point energy correction to the barrier height (ΔZPE) is defined as the ZPE of the transition state minus the ZPE of the minimum.

To illustrate the expense of using QM methods for conformational analysis, an energy-directed tree search algorithm (EDTS)[42] in conjunction with a computationally less expensive density functional theory model, PBE0/cc-pVTZ,[43] was used to conduct a conformer search of **7**. Nine unique minima identified in this search were subsequently optimized at the MP2/cc-pVTZ level of theory.

Cambridge Structural Database. Average experimental structural parameters (bond lengths and bond angles) and dihedral angle distributions were obtained through analysis of the Cambridge Structural Database (CSD).[44,45] The CSD program ConQuest was used to identify crystal structures containing different subsets of organophosphine oxide molecules, OPR_3. In all searches, the PO oxygen atom was constrained to have a coordination number of one (to avoid protonated or metal coordinated examples), and all bonds to P were constrained to be acyclic (to avoid cases where the P atom was incorporated within a ring system). All searches were subjected to the following filters: 3D coordinates determined, R factor ≤0.1, not disordered, no errors, no powder structures.

Three series of searches were performed. To obtain data for comparison of bond length and bond angle data to computed values, the first series of searches were constrained so that P was attached to two methyl substituents, with the third substituent being either a methyl, ethyl, isopropyl, *tert*-butyl, vinyl, or phenyl group. These searches located four examples of **1** and one example of **6**. Loosening these criteria so that the first two substituents could be either $-CH_3$ or $-CH_2C$ (representing any primary alkyl), and the second substituent could be $-CH_2C$, $-CHC_2$ (secondary alkyl), $-CC_3$ (tertiary alkyl), or a vinyl group, a second series of searches yielded 21 analogues of **2**, two analogues of **3**, and two analogues of **4**, and no analogues of **5**. Loosening the criteria even further to allow the first two substituents to be any four coordinate carbon group, a third series of searches were performed to obtain dihedral angle data distributions in analogues of **1**−**6** giving (rotor group, number of crystal structures): $-CH_3$, 40; $-CH_2C$, 31; $-CHC_2$, 15; $-CC_3$, 7; vinyl, 0; phenyl, 22. Diagrams of the CSD search fragments are provided as Supporting Information.

Force Field Calculations. After comparing the performance of the existing Merck Molecular Force Field 94 (MMFF94)[46−52] and MM3[35] models in PCModel,[53] the MM3 model was chosen since it has the best default performance (see Supporting Information for the MMFF94 data). Calculations were performed with the MM3 force field[35] as implemented in the PCModel molecular modeling software.[53] MP2/cc-pVTZ optimized geometries for **1**−**6** and crystal structure data provided a basis for both testing the ability of the prior MM3 model[37,38] to predict bond lengths and angles in **1**−**4** as well as the assignment of bond length and angle parameters for **5** and **6**. After ensuring that bonds and angles were well-reproduced, torsional parameters for X−P−C−Y dihedral angles (X = C, O; Y = C, H) were adjusted to give the best fit to rotational PESs. The final set of updated parameters is provided as Supporting Information. In the ensuing discussion, this model is termed MM3+ to distinguish it from the default MM3 model. The performance of MM3+ was tested by evaluation of **7** and **8**, including a conformational search of **7** using PCModel's GMMX algorithm.

RESULTS AND DISCUSSION

The conformations of a series of RMe_2PO molecules were evaluated at the MP2/cc-pVTZ level of theory. PESs for the rotation of the methyl group (Me) in **1**, ethyl group in **2**, isopropyl group in **3**, *tert*-butyl group in **4**, vinyl group in **5**, and phenyl group in **6** were determined. Because the Me substituents in **1**−**6** each exhibit only one 3-fold degenerate

DOI: 10.1021/acs.jpca.5b04687
J. Phys. Chem. A 2015, 119, 8765−8773

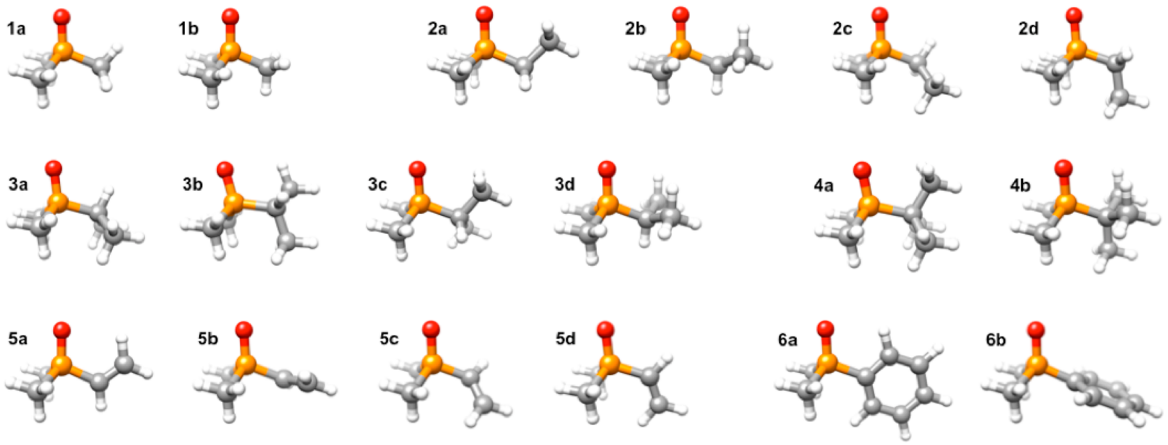

Figure 1. MP2/cc-pVTZ optimized geometries for all stationary points in the rotational PESs for **1**−**6** shown in Figures 2−7.

rotamer, these PESs identified the approximate location for all minima of each molecule as well as the transition states for the P−C bond that was rotated. Views of the fully optimized geometries for these transition states and minima are presented in Figure 1, and their relative energies, with and without ZPE corrections, are summarized in Table 1. These results were used

Table 1. Summary of Stationary Points on Rotational PESs for 1−6[a]

stationary point	ϕ (deg)	ν (cm^{-1})	E_{rel} without ZPE (kcal/mol)	E_{rel} with ZPE(kcal/mol)
1a	0.0	196*i*	2.2	2.0
1b	59.1	153	0.0	0.0
2a	0.0	92*i*	2.4	2.4
2b	54.6	75	0.0	0.0
2c	119.2	101*i*	3.4	3.5
2d	180.0	53	0.6	0.6
3a	0.0	80*i*	4.6	4.8
3b	62.2	39	0.4	0.4
3c	118.8	76*i*	3.6	3.7
3d	180.0	52	0.0	0.0
4a	0.0	77*i*	4.8	5.1
4b	58.4	16	0.0	0.0
5a	0.0	98	0.0	0.0
5b	70.0	96*i*	3.5	3.2
5c	126.6	75	2.1	2.1
5d	180.0	50*i*	2.8	2.5
6a	0.0	45	0.0	0.0
6b	87.9	38*i*	2.9	2.9

[a]Results reported in this table were obtained at the MP2/cc-pVTZ level of theory. Stationary point labels correspond to transition states and minima in PESs shown in Figures 2−7. ϕ is the O═P−C−X torsion angle (X = C or H) obtained after geometry optimization. ν is the lowest frequency for the minima or the single imaginary frequency for the transition states. E_{rel} is the electronic energy relative to the lowest energy structure for a given molecule. ZPE = zero point energy.

to improve and extend the prior MM3 model. The process involved first adjusting bond length and angle parameters followed by assignment of torsion parameters.

Bond Lengths and Angles. MP2 bond lengths and angles for the most stable geometries in **1**−**6** are compared with average experimental values observed in crystal structures in Table 2. Search of the CSD provided crystals that explicitly contained **1** and **6**, allowing an exact comparison in the structures between the CSD and the gas phase computations for **1** and **6**. Repeating the searches using analogous structures in which the Me groups attached to phosphorus were allowed to be any primary alkyl group and Me groups on the rotating alkyl substituent were allowed to be any alkyl group provided data for comparison to **2**−**4**. No such data were available for **5**. Where possible, Table 2 also summarizes bond lengths and angles obtained after geometry optimization using the MM3 and MM3+ models.

Experimental PO bond lengths, which are relatively insensitive to the nature of the carbon substituents, are reproduced within 0.005 Å by all three models. The P−C (where the C is four-coordinate) bond lengths exhibit the expected trend of increasing with increasing steric bulk as α hydrogen groups are replaced by α carbon groups. On going from methyl to a tertiary substituent, the mean bond length values in crystal structures increase from 1.79 to 1.84 Å and in MP2 optimized geometries from 1.81 to 1.84 Å. This effect is mimicked in the MM3 models where the elongated lengths result from both increased steric repulsion between P substituents and electronegativity corrections that increase the ideal P−C bond length as α hydrogen groups are replaced by α carbon groups. Experimental P−C bond lengths are reproduced to within an average absolute error of 0.011 Å with MP2, 0.017 Å with MM3, and 0.014 Å with MM3+. The MM3+ values reproduce the MP2 values with an average absolute error of 0.004 Å. The maximum error in P−C bond lengths are 0.023 Å with MP2, 0.030 Å with MM3, and 0.027 Å with MM3+.

Comparison with experimental bond angles subtended at P reveals that the MP2 model systematically overestimates O═P−C angles by an average of 1.3° (with 2.0° maximum error) and underestimates C−P−C angles by an average of −1.4° (with −2.3° maximum error). The prior MM3 model gives similar trends, with O═P−C angles that are too high by an average of 1.6° (with 3.2° maximum error) and C−P−C angles that are low by −1.4° (with −2.6° maximum error). After adjusting bending parameters in MM3+, it was possible to reduce discrepancies with experimentally observed values to within an average errors of −0.4 (with −1.8° maximum error) and 0.9° (with 2.0° maximum error) in O═P−C and C−P−C angles, respectively.

Rotational PESs. Data for rotation about P−C bonds in **1**−**6** are summarized in Figures 2−7, respectively. Where possible,

DOI: 10.1021/acs.jpca.5b04687
J. Phys. Chem. A 2015, 119, 8765−8773

Table 2. Comparison of Bond Lengths (Å) and Angles (deg) from X-ray Data and Optimized Global Minimum Geometries for 1−6 at the MP2, MM3, and MM3+ Levels of Theory

no.	feature[a]	X-ray[b]	MP2	MM3	MM3+
1b	P═O	1.489 ± 0.001	1.484	1.490	1.490
	$P-C_{Me}$	1.785 ± 0.011	1.808	1.815	1.812
	$O═P-C_{Me}$	112.9 ± 0.6	114.3	114.0	112.1
	$C_{Me}-P-C_{Me}$	105.8 ± 0.7	104.3	104.6	106.7
2b	P═O	1.494 ± 0.016	1.486	1.490	1.490
	$P-C_{1°}$	1.807 ± 0.013	1.814	1.825	1.822
	$P-C_X$	1.804 ± 0.017	1.809	1.816	1.813
	$O═P-C_{1°}$	112.9 ± 1.5	113.8	114.1	112.4
	$O═P-C_X$	112.9 ± 1.2	114.5	113.8	111.8
	$C_{1°}-P-C_X$	105.8 ± 1.3	104.7	104.8	107.0
	C_X-P-C_X	105.7 ± 1.4	104.1	104.1	106.3
3d	P═O	1.488 ± 0.017	1.488	1.490	1.490
	$P-C_{2°}$	1.829 ± 0.001	1.824	1.839	1.836
	$P-C_X$	1.796 ± 0.003	1.810	1.817	1.814
	$O═P-C_{2°}$	112.0 ± 0.1	113.4	114.2	112.5
	$O═P-C_X$	112.2 ± 0.1	114.2	113.8	111.9
	$C_{2°}-P-C_X$	107.5 ± 0.5	105.2	105.4	107.3
	C_X-P-C_X	105.0 ± 1.2	103.5	103.2	105.5
4b	P═O	1.490 ± 0.002	1.488	1.490	1.490
	$P-C_{3°}$	1.850 ± 0.028	1.836	1.839	1.836
	$P-C_X$	1.797 ± 0.004	1.811	1.817	1.814
	$O═P-C_{3°}$	111.0 ± 0.4	112.4	114.2	112.5
	$O═P-C_X$	113.1 ± 1.0	113.6	113.8	111.9
	$C_{3°}-P-C_X$	106.8 ± 0.6	106.6	107.0	108.8
	C_X-P-C_X	105.7 ± 1.5	103.4	103.1	105.7
5a	P═O		1.486		1.489
	$P-C_V$		1.799		1.811
	$P-C_{Me}$		1.807		1.801
	$O═P-C_V$		113.5		112.3
	$O═P-C_{Me}$		114.7		112.2
	C_V-P-C_{Me}		104.2		106.2
	$C_{Me}-P-C_{Me}$		104.2		107.3
6a	P═O	1.492	1.486		1.490
	$P-C_{Ph}$	1.810	1.809		1.810
	$P-C_{Me}$	1.792	1.807		1.812
	$O═P-C_{Ph}$	111.3	112.9		111.5
	$O═P-C_{Me}$	113.6	114.5		111.8
	$C_{Ph}-P-C_{Me}$	105.8	104.7		106.8
	$C_{Me}-P-C_{Me}$	105.9	104.5		107.7

[a]Nomenclature: Me = CH_3; 1° = CH_2R; 2° = CHR_2; 3° = CR_3; V = vinyl; Ph = phenyl; X = either CH_3 or CH_2R (R = any substituent attached by a carbon atom). [b]Mean observed values from the CSD. Uncertainties represent one sample standard deviation.

each figure gives the rotational PES obtained using the MP2/cc-pVTZ, MM3, and MM3+ model. These energy profiles were obtained by constraining the O═P−C−X dihedral angle (X = H for **1** and **3**, C for **2** and **4**−**6**) at intervals of 5° from 0 to 360° and fully optimizing the remaining degrees of freedom. Labels, consisting of a lower case alphabetical letter added to the molecule number, are used to reference the transition states and minima shown in Figure 1. In addition, with the exception of **5** for which there was a lack of data, the theoretical energy profiles are compared with dihedral angle distributions observed for molecular analogues in the solid state.

Rotation of tetrahedral carbon substituents attached to a tetrahedral P atom gives rise to the expected staggered

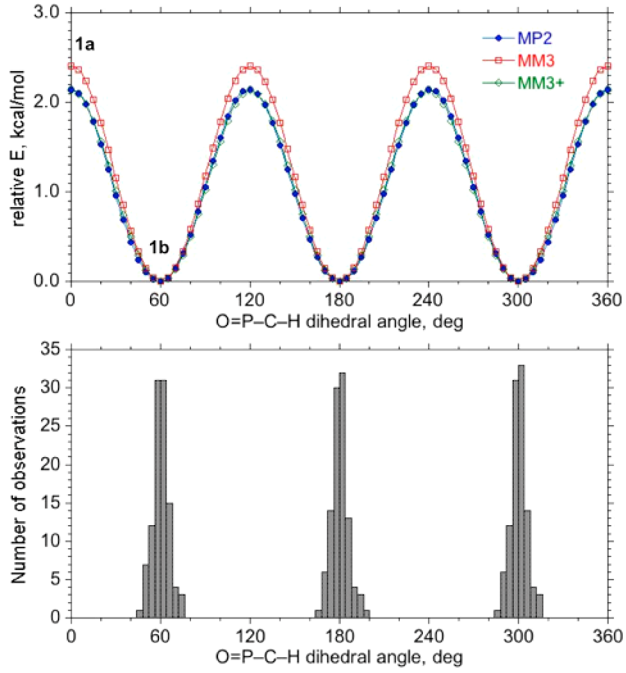

Figure 2. Comparison of MP2, MM3, and MM3+ PESs for rotation of a single methyl group in **1** (top) with the experimental distribution of O═P−C−H dihedral angles about P−Me bonds in crystal structures containing OPR_2Me, where R is any alkyl group (bottom). Geometries associated with labeled transition state, **1a**, and minimum, **1b**, are shown in Figure 1.

minimum configurations, in other words, *trans* (180°) and *gauche* (±60°) rotamers with transition states located near 0° and ±120°. Methyl rotation in **1** (Figure 2) and *tert*-butyl rotation in **4** (Figure 5) yield PESs that exhibit three equivalent minima, geometries **1b** and **4b**, respectively. Ethyl rotation in **2** (Figure 3) and isopropyl rotation in **3** (Figure 4) yield PESs characterized by two energetically equivalent minima, one near +60°, **2b** and **3b**, and one (mirror image) near −60°, and one unique minimum near 180°, **2d** and **3d**. The observed stability order can be predicted by identifying the form that minimizes the extent of steric repulsion between adjacent rotor substituents, which is expected to decrease in the following order: Me(P), Me(C) > O(P), Me(C) > Me(P), H(C) > O(P), H(C). In both **2** and **3**, the more stable form is the orientation that places a small hydrogen atom substituent on the α carbon of the rotating alkyl group in between the two Me groups on the P atom, **2b** and **3d**.

As seen in Table 1, torsional barriers in **1**−**4** tend to increase with the steric bulk of the rotating alkyl group. In addition, the frequency of the torsional mode of the lowest energy minima decreases as the rotating group gets bulkier: 153 > 75 > 52 > 16 cm^{-1} for **1**−**4**, respectively. The imaginary frequencies of the high-energy transition states also decrease in the same order, but with a somewhat higher magnitude $196i > 101i > 80i > 77i$ cm^{-1}. These trends in the frequencies show that the region near the top of the barrier is tighter (more narrow along the rotation coordinate) than the region near the minimum. The MP2 rotational barriers are essentially unaffected by zero-point corrections.

Vinyl group rotation in **5** (Figure 6) yields a PES showing one minimum at 0°, **5a**, and two higher energy minima, one near +125°, **5c**, and its mirror image at −125°. In these minima, the double bond is eclipsed and the α H atom is staggered with

DOI: 10.1021/acs.jpca.5b04687
J. Phys. Chem. A 2015, 119, 8765−8773

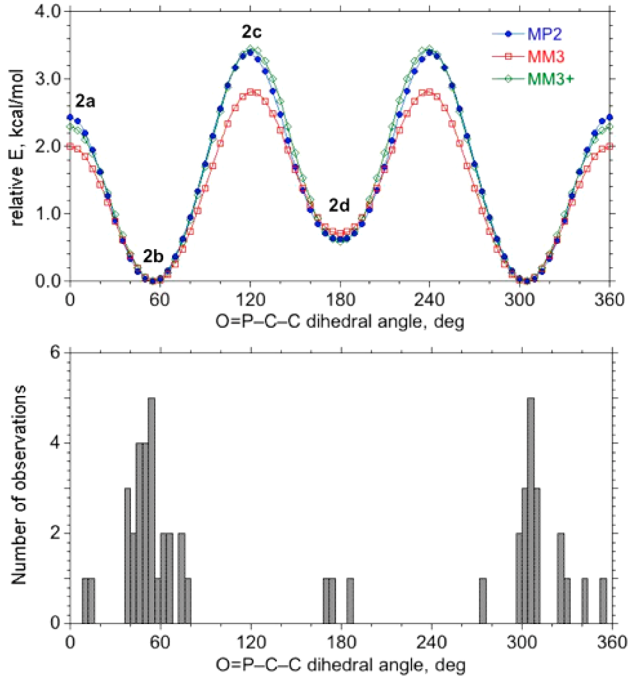

Figure 3. Comparison of MP2, MM3, and MM3+ PESs for ethyl group rotation in **2** (top) with the experimental distribution of O═P−C−C dihedral angles about P−CH_2R' bonds in crystal structures containing $OPR_2(CH_2R')$, where R is any alkyl group and R′ is any group attached by a carbon atom (bottom). Geometries associated with labeled transition states, **2a** and **2c**, and minima, **2b** and **2d**, are shown in Figure 1.

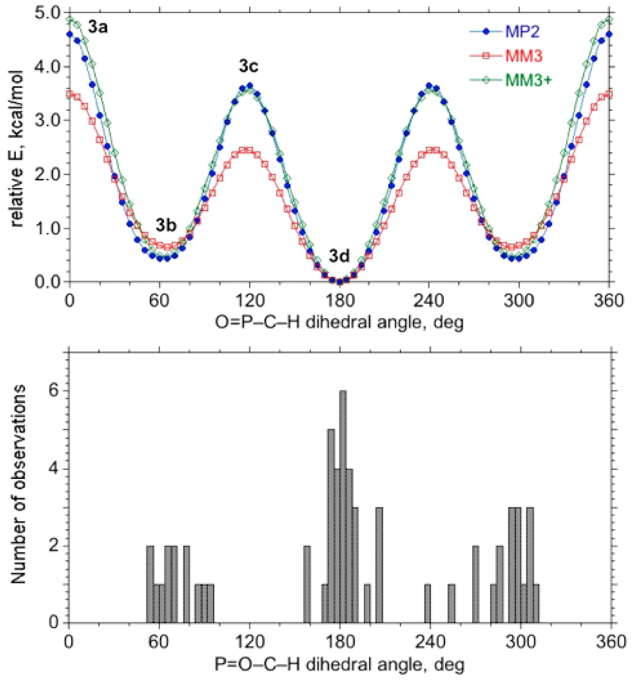

Figure 4. Comparison of MP2, MM3, and MM3+ PESs for isopropyl group rotation in **3** (top) with the experimental distribution of O═P−C−H dihedral angles about P−CHR′R″ bonds in crystal structures containing $OPR_2(CHR'R'')$, where R is any alkyl group and R′ and R″ are any group attached by a carbon atom (bottom). Geometries associated with labeled transition states, **3a** and **3c**, and minima, **3b** and **3d**, are shown in Figure 1.

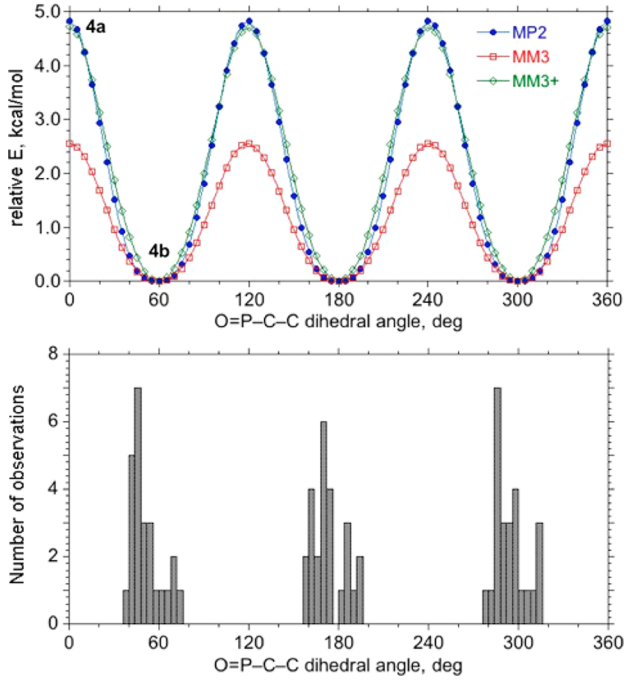

Figure 5. Comparison of MP2, MM3, and MM3+ PESs for *tert*-butyl group rotation in **4** (top) with the experimental distribution of O═P−C−C dihedral angles about P−CR′R″R‴ bonds in crystal structures containing $OPR_2(CR'R''R''')$, where R is any alkyl group and R′, R″, and R‴ are any group attached by a carbon atom (bottom). Geometries associated with labeled transition state, **4a**, and minimum, **4b**, are shown in Figure 1.

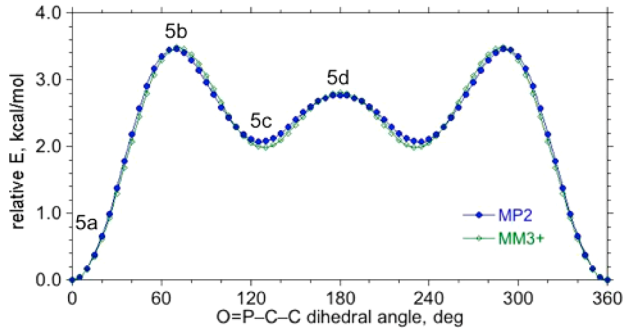

Figure 6. MP2 and MM3+ PESs for vinyl group rotation in **5**. Geometries associated with labeled minima, **5a** and **5c**, and transition states, **5b** and **5d**, are shown in Figure 1.

respect to the P substituents. At 180°, the height of the barrier between the two high-energy forms is 0.4 kcal/mol after zero point energy correction (Table 1), below the thermal energy value, kT = 0.6 kcal/mol at 298 K, indicating that these two forms are freely interconverting at room temperature. Phenyl group rotation in **6** (Figure 7) yields a PES with two equivalent minima at 0° and 180°, **6a**. In this minimum the plane of the phenyl ring is eclipsed with the P═O bond and lies in between the two Me groups attached to the P atom. As with the alkyl substituents, zero point energy corrections have a small impact on the barrier heights.

The rotational PESs are compared with dihedral angle distributions observed for methyl (−CH_3, Figure 2), primary alkyl (−CH_2C, Figure 3), secondary alkyl (−CHC_2, Figure 4), tertiary alkyl (−CC_3, Figure 5), and phenyl (C_6 arenes with two ortho H atoms, Figure 7) rotors on phosphine oxides

DOI: 10.1021/acs.jpca.5b04687
J. Phys. Chem. A 2015, 119, 8765−8773

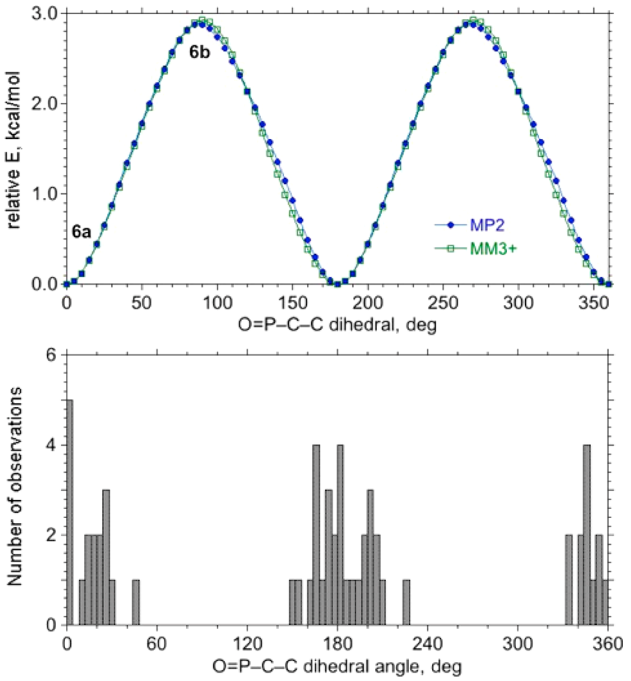

Figure 7. Comparison of MP2 and MM3+ PESs for phenyl group rotation in **6** (top) with the experimental distribution of O=P–C–C dihedral angles about P–Ph bonds in crystal structures containing OPR_2Ph, where R is any alkyl group (bottom). Geometries associated with labeled minimum, **6a**, and transition state, **6b**, are shown in Figure 1.

substituted with two additional alkyl groups. In every case, the experimental distribution is consistent with the theoretical PES. In other words, the dihedral angles observed in crystal structures cluster in regions corresponding to minima in the gas-phase PESs; when there are two distinct minima of differing energy, as with **2** and **3**, there is more crystal structure data available associated with the lower energy minimum than the higher energy one.

Figures 2–7 also provide a comparison of the PESs obtained with the MM3 and MM3+ models. With **1**–**4**, MM3 does a good job predicting the location and relative energy of the minima. However, it slightly overestimates barrier heights in **1** and significantly underestimates barrier heights in **2**–**4**. After adjustment of torsional parameters to fit the MP2 PESs, these discrepancies are minimized in MM3+. While these changes in the parameters for MM3+ make only small improvements to the location and relative energies of the minima (the largest changes are for the minima of **2** and **3**), there are significant changes to the energetics of the maxima and therefore the shape of the potential energy surfaces away from the minima. This would have an effect on molecular dynamics simulations or in other situations where the molecule must distort away from the minimum geometry. Similarly, after the adjustment of torsional parameters in new terms added to treat unsaturated substituents, it was possible to obtain close agreement between the MP2 and MM3+ PES for **5** and **6**. Overall, the dihedral angles for all MM3+ stationary points are within 3° of the dihedral angles of MP2 stationary points, and relative MP2 energies for all minima and transition states are reproduced to within 0.3 kcal/mol by MM3+.

Conformational Analysis of 7. As mentioned in the Introduction, there are times when it is much more efficient to use a force field model than an electronic structure model to solve a problem. An example occurs when conducting a conformational search, which typically involves the optimization of a large number of trial structures in order to locate all low-energy conformers. Even with a relatively simple molecule, such as **7**, this process can be time-consuming if done using QM. To illustrate this point, the EDTS algorithm was used with the PBE0/cc-pVTZ model to perform a conformational search of **7**. This search, which required 3200 CPU hours, yielded nine unique minima. Further geometry optimization and frequency calculations at the MP2/cc-pVTZ level of theory, which required an additional 4800 CPU hours, yielded the geometries for **7a**–**7i** shown in Figure 8. Relative energies are summarized in Table 3.

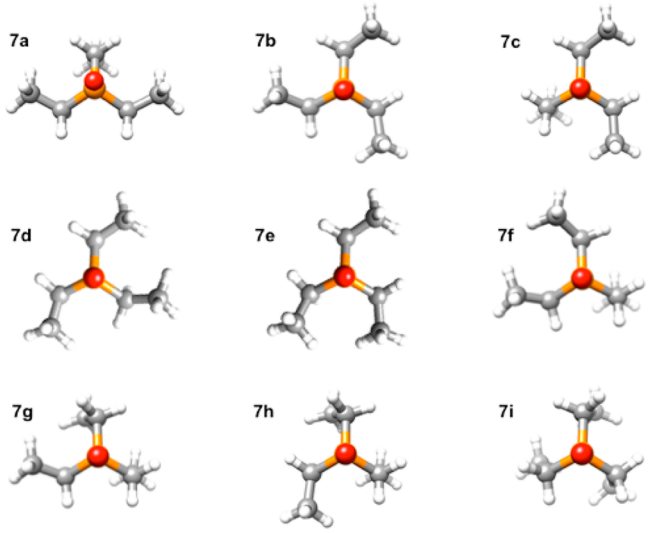

Figure 8. MP2/cc-pVTZ optimized geometries for the nine unique minima for **7**.

Table 3. Relative Energies (kcal/mol) for Conformers of 7

conformer[a]	MP2	MM3+	conformer[a]	MP2	MM3+
7a	0.00	0.33	**7f**	1.44	1.38
7b	0.04	0.00	**7g**	2.27	2.54
7c	0.27	0.37	**7h**	2.33	2.60
7d	0.88	1.12	**7i**	5.00	5.55
7e	0.98	1.07			

[a]See Figure 8.

Repeating the conformer search using the GMMX algorithm and the MM3+ model identified the same nine conformations in 70 seconds of CPU time. Comparison of the relative energies obtained with MP2 versus those obtained with MM3+ (Table 3) reveals an average absolute error of only 0.2 kcal/mol. Thus, the force field model gives essentially the same result with respect to geometry and relative energy, but does it 2×10^5 times faster (including both the PBE and MP2 computations, but excluding the MP2 Hessian calculations).

The conformational search results indicate that the MM3+ model, which was derived by fitting data to **1**–**6**, is transferable to other organophosphine oxides. The extent of this transferability is further probed by comparing the PES obtained by rotation of one ethyl groups in the C_3 symmetric conformer, **7b**. The comparison, shown in Figure 9, illustrates that although there is not a perfect correspondence, the MM3+ model does predict the presence of four minima and four

DOI: 10.1021/acs.jpca.5b04687
J. Phys. Chem. A 2015, 119, 8765–8773

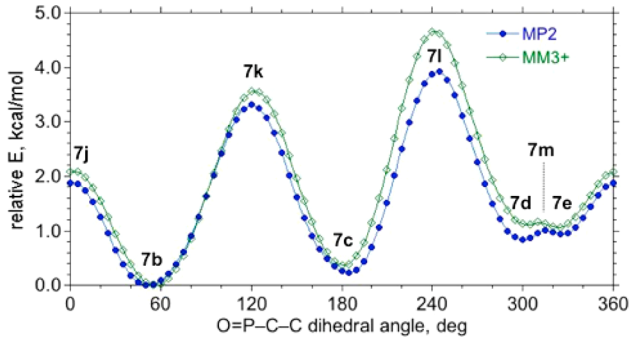

Figure 9. Comparison of MP2 and MM3+ PESs obtained for rotation about one of the P−C bonds in **7b**. Geometries associated with labeled minima, **7b**−**e**, are shown in Figure 8.

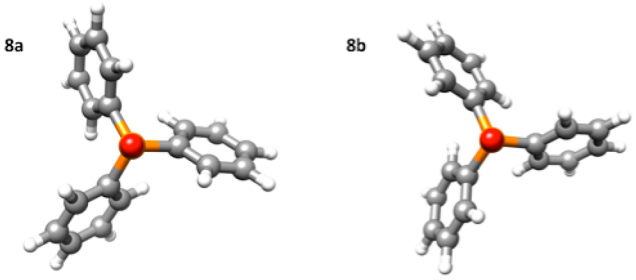

Figure 10. MP2/cc-pVTZ optimized geometries for the two stereoisomers of **8**.

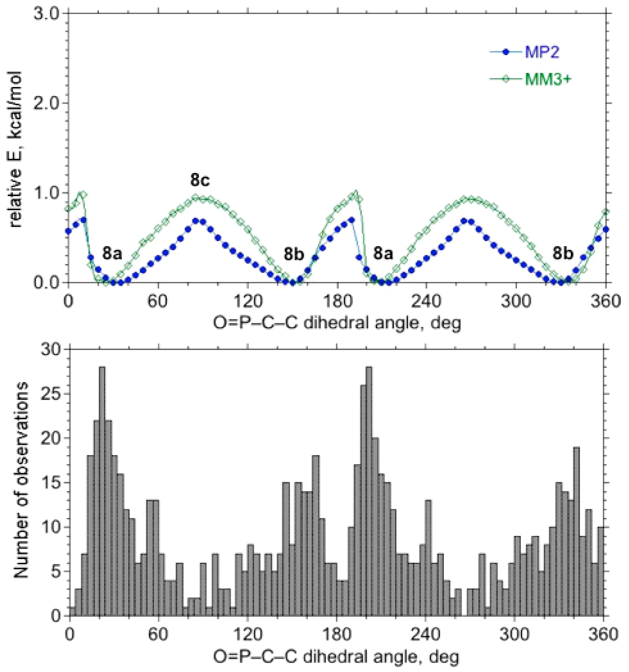

Figure 11. Comparison of MP2 and MM3+ PESs obtained for rotation about one of the P−C bonds in **8** (top) with the experimental distribution of O═P−C−C dihedral angles in crystal structures containing O═PPh_3 (bottom). Geometries associated with labeled minima, **8a,b**, are shown in Figure 10.

transition states, reproducing the surface to within an average absolute deviation of 0.3 kcal/mol. The transition states associated with Figure 9 are available in the Supporting Information.

Conformational Analysis of 8. Triphenylphosphine oxide, **8**, is often used to help induce crystallization,[54] and as a result, there are 128 crystal structure examples in the CSD containing non-metal-coordinated examples of **8**. An MM3+ conformer search of this molecule yields only the two energetically equivalent C_3 symmetric minima shown in Figure 10, **8a** and **8b**, which are mirror images of one another. When a rotational PES is generated by constraining the dihedral angle of one of the phenyl groups in **8**, the molecule changes chirality three times on going from 0 to 360°. Comparison of the PESs obtained with MP2 and MM3+ (Figure 11) shows that the two levels of theory yield similar energy profiles, with MM3+ giving an average absolute deviation from the MP2 energies of 0.22 kcal/mol. The O═P−C−C dihedral angle at the minima is predicted to be ±33° by MP2 and ±25° by MM3+. The calculated degree of twist in the phenyl groups is in good agreement with the distribution of dihedral angles observed in X-ray structures. The experimental distribution of dihedral angles is concentrated in the regions ±(15−30°) on either side of 0° and 180°. The PESs show what seem like two different transition states. One of them occurs near 90° and 270°, and the other occurs near 0° and 180°. The discontinuity in the PES for the latter one is caused when a phenyl group that is adjacent to the one being driven undergoes a large rotation, flipping over 90°. This adjacent phenyl group is close to perpendicular to the axis of the PO bond before the large rotation occurs, making the structure similar to the one at 90° and 270° in Figure 11. When the two structures transition states are fully optimized with no constraints, it is clear that the two structures are identical, **8c** (available in Supporting Information).

It is interesting to compare the PES shown in Figure 11 for phenyl rotation in **8** with that in Figure 7 for phenyl rotation in **6**. Replacing the two methyl substituents in **6** with two phenyl substituents in **8** results in a significant decrease in the MP2 barrier height from 2.9 to 0.7 kcal/mol. The fact that the MM3+ model predicts this decrease indicates that the change in barrier height is primarily due to differences in steric and electrostatics interactions, rather than other possible causes, such as induction effects or $\pi-\pi$ interactions, neither of which are explicitly treated by terms in the force field model.

SUMMARY

Geometric and energetic data were computed for a series of organophosphine oxides, $OP(Me)_2R$ (**1**−**6**), at the MP2/cc-pVTZ level of theory. The accuracy of this model was assessed by comparison of the calculated structures with those observed in crystal structures. The mean absolute deviations between theory and experimental structural features are 0.005 Å for O═P distance, 0.011 Å for P−C distance, 1.3° for O═P−C angle, and 1.4° for C−P−C angle. The gas phase PESs for rotation about the P−C bond for representative R groups (methyl, ethyl, isopropyl, *tert*-butyl, and phenyl) are consistent with experimental dihedral angle distributions, correctly predicting the location and relative abundance of observed rotamers in the solid state.

The stability of conformers can be predicted by minimizing the amount of steric repulsion between adjacent, alkyl rotor substituents: Me(P), Me(C) > O(P), Me(C) > Me(P), H(C) > O(P), H(C). In addition, the torsional barriers for the alkyls increase with the steric bulk of the rotating group. The imaginary frequencies associated with the high-energy transition states ($196i$ > $101i$ > $80i$ > $77i$ cm^{-1}), and the real

DOI: 10.1021/acs.jpca.5b04687
J. Phys. Chem. A 2015, 119, 8765−8773

frequencies associated with torsional motion of the lowest energy minima (153 > 75 > 52 > 16 cm^{-1}) decrease as the rotating group gets bulkier. The differences in the magnitudes of the frequencies in the transition states and minim show that the top of the barrier is tighter than near the minima.

The MM3 force field was adjusted and extended to reproduce the above results (MM3+), yielding a fast and accurate model for predicting the shapes of OPR_3 molecules. The transferability of this model was illustrated by the conformational analysis of two additional compounds: triethylphosphine oxide, **7**, and triphenylphosphine oxide, **8**. In both cases, MM3+ yields results that closely mimic those obtained with MP2 but does so in a fraction of the time. For example, although **7** is a relatively simple molecule, the time taken to perform an exhaustive conformational analysis using QM methods and obtain the final result consisting of nine unique conformers rank ordered by MP2 energy was almost half a CPU year. A comparable result was obtained in little over 1 CPU minute using the MM3+ model.

■ ASSOCIATED CONTENT

Ⓢ Supporting Information

Cartesian coordinates and absolute energies for all MP2/cc-pVTZ optimized structures, table of MM3+ force field parameters, diagrams of the molecular fragments used in Cambridge Database Searches, and MMFF94 comparisons for structures **1**−**6**. The Supporting Information is available free of charge on the ACS Publications website at DOI: 10.1021/acs.jpca.5b04687.

■ AUTHOR INFORMATION

Corresponding Author

*Phone (515)-294-6134; Fax (515) 294-0105; e-mail twindus@iastate.edu (T.L.W.).

Notes

The authors declare no competing financial interest.

■ ACKNOWLEDGMENTS

This work is supported by the Critical Materials Institute, an Energy Innovation Hub funded by the U.S. Department of Energy, Office of Energy Efficiency and Renewable Energy, Advanced Manufacturing Office. This research used resources of the Oak Ridge Leadership Computing Facility at the Oak Ridge National Laboratory, which is supported by the Office of Science of the U.S. Department of Energy under Contract DE-AC05-00OR22725.

■ REFERENCES

(1) Corbridge, D. E. C. *Phosphorus: An Outline of Its Chemistry, Biochemistry, and Technology*; Elsevier: Amsterdam, 1995.

(2) Schmidt, M. W.; Gordon, M. S. Electronic-Structure of the Phosphoryl and Thiophosphoryl Bonds. *J. Am. Chem. Soc.* **1985**, *107*, 1922−1930.

(3) Chesnut, D. B.; Savin, A. The Electron Localization Function (ELF) Description of the PO Bond in Phosphine Oxide. *J. Am. Chem. Soc.* **1999**, *121*, 2335−2336.

(4) Chesnut, D. B. Atoms-in-Molecules and Electron Localization Function Study of the Phosphoryl Bond. *J. Phys. Chem. A* **2003**, *107*, 4307−4313.

(5) De Silva, N.; West, A. C.; Windus, T. L.; Gordon, M. S. Manuscript in preparation.

(6) Shabana, R.; Ruf, H. Extraction and Separation of Neptunium, Uranium, Thorium and Cerium with Topo from Mixed-Solvents. *Radiochim. Acta* **1976**, *23*, 117−120.

(7) Manh, T. N.; Kopunec, R. Carrier-Mediated Transport of Rare-Earth Elements through Liquid Membranes - Transport of Sc, Y, Ce, Eu, Gd, Tm, Yb through Supported Liquid Membrane Containing TOPO in N-Dodecane. *J. Radioanal. Nucl. Chem.* **1992**, *159*, 219−231.

(8) Mathur, J. N.; Choppin, G. R. Paraffin Wax - TOPO, an Extractant for Actinides and Lanthanides. *Solvent Extr. Ion Exch.* **1998**, *16*, 739−749.

(9) Turanov, A. N.; Karandashev, V. K.; Baulin, V. E.; Yarkevich, A. N.; Safronova, Z. V. Extraction of Lanthanides(iii) from Aqueous Nitrate Media with Tetra-(p-tolyl)[(o-phenylene)Oxymethylene] Diphosphine Dioxide. *Solvent Extr. Ion Exch.* **2009**, *27*, 551−578.

(10) Dudwadkar, N. L.; Tripathi, S. C.; Dhami, P. S.; Gandhi, P. M. Partitioning of Actinides from High-Level Liquid Waste Employing Supported Liquid Membrane Technique Using TOPO in N-Dodecane as Carrier. *Desalin. Water Treat.* **2014**, *52*, 4755−4761.

(11) Xie, F.; Zhang, T. A.; Dreisinger, D.; Doyle, F. A Critical Review on Solvent Extraction of Rare Earths from Aqueous Solutions. *Miner. Eng.* **2014**, *56*, 10−28.

(12) Rout, A.; Binnemans, K. Influence of the Ionic Liquid Cation on the Solvent Extraction of Trivalent Rare-Earth Ions by Mixtures of Cyanex 923 and Ionic Liquids. *Dalton Trans.* **2015**, *44*, 1379−1387.

(13) Egan, B. Z.; Lee, D. D.; Mcwhirter, D. A. Solvent-Extraction and Recovery of Ethanol from Aqueous-Solutions. *Ind. Eng. Chem. Res.* **1988**, *27*, 1330−1332.

(14) Watson, E. K.; Rickelton, W. A.; Robertson, A. J.; Brown, T. J. A Liquid Phosphine Oxide - Solvent-Extraction of Phenol, Acetic-Acid and Ethanol. *Solvent Extr. Ion Exch.* **1988**, *6*, 207−220.

(15) Beltrami, D.; Cote, G.; Mokhtari, H.; Courtaud, B.; Moyer, B. A.; Chagnest, A. Recovery of Uranium from Wet Phosphoric Acid by Solvent Extraction Processes. *Chem. Rev.* **2014**, *114*, 12002−12023.

(16) Watson, E. K.; Rickelton, W. A. A Review of the Industrial and Recent Potential Applications of Trioctylphosphine Oxide. *Solvent Extr. Ion Exch.* **1992**, *10*, 879−889.

(17) Safiulina, A. M.; Matveeva, A. G.; Dvoryanchikova, T. K.; Sinegribova, O. A.; Tu, A. M.; Tatarinov, D. A.; Kostin, A. A.; Mironov, V. F.; Tananaev, I. G. Acetyl-Containing Phosphine Oxides as Extractants for Actinides and Lanthanides. *Russ. Chem. Bull.* **2012**, *61*, 392−398.

(18) Sasaki, Y.; Kitatsuji, Y.; Sugo, Y.; Tsubata, Y.; Kimura, T.; Morita, Y. Actinides Extractability Trends for Multidentate Diamides and Phosphine Oxides. *Solvent Extr. Res. Dev., Jpn.* **2012**, *19*, 51−61.

(19) Fang, Y. Y.; Wu, L.; Liao, J. L.; Chen, L.; Yang, Y. Y.; Liu, N.; He, L. T.; Zou, S. L.; Feng, W.; Yuan, L. H. Pillar[5]Arene-Based Phosphine Oxides: Novel Ionophores for Solvent Extraction Separation of f-Block Elements from Acidic Media. *RSC Adv.* **2013**, *3*, 12376−12383.

(20) Lukashova, M. S.; Belikov, K. N.; Bryleva, K. Y.; Verbytska, A. V.; Kal'chenko, V. I. Effect of the Structure of Calix[4]Arenes, Containing Phosphine Oxide and Phosphoryl Groups and Impregnated on Silica Gel, on the Efficiency of Eu^{3+} Extraction from Aqueous Solutions. *Theor. Exp. Chem.* **2013**, *49*, 199−203.

(21) Rosario-Amorin, D.; Ouizem, S.; Dickie, D. A.; Paine, R. T.; Cramer, R. E.; Hay, B. P.; Podair, J.; Delmau, L. H. Synthesis and Lanthanide Coordination Chemistry of Phosphine Oxide Decorated Dibenzothiophene and Dibenzothiophene Sulfone Platforms. *Inorg. Chem.* **2014**, *53*, 5698−5711.

(22) Boyd, D. R.; Bell, M.; Dunne, K. S.; Kelly, B.; Stevenson, P. J.; Malone, J. F.; Allen, C. C. R. Chemoenzymatic Synthesis of a Mixed Phosphine-Phosphine Oxide Catalyst and Its Application to Asymmetric Allylation of Aldehydes and Hydrogenation of Alkenes. *Org. Biomol. Chem.* **2012**, *10*, 1388−1395.

(23) Chen, J. Z.; Liu, D. L.; Fan, D. Y.; Liu, Y. G.; Zhang, W. B. Synthesis of Axially Chiral C-10-Bridgephos Oxides and Their Use as Organocatalysts in Enantioselective Allylations of Aldehydes. *Tetrahedron* **2013**, *69*, 8161−8168.

(24) Kotani, S.; Sugiura, M.; Nakajima, M. Eccnouantntioselective Double Aldol Reactions Involving the Sequential Activation of Silicon Tetrachloride by Chiral Phosphine Oxides. *Synlett* **2014**, *25*, 631−640.

DOI: 10.1021/acs.jpca.5b04687
J. Phys. Chem. A 2015, 119, 8765−8773

(25) Lam, K. H.; Chui, C. H.; Gambari, R.; Wong, R. S. M.; Cheng, G. Y. M.; Lau, F. Y.; Lai, P. B. S.; Tong, S. W.; Chan, K. W.; Wong, W. Y.; Chan, A. S. C.; Tang, J. C. O. The Preparation of Bi-Functional Organophosphine Oxides as Potential Antitumor Agents. *Eur. J. Med. Chem.* **2010**, *45*, 5527−5530.
(26) Jeon, S. O.; Lee, J. Y. Phosphine Oxide Derivatives for Organic Light Emitting Diodes. *J. Mater. Chem.* **2012**, *22*, 4233−4243.
(27) Liu, X. K.; Zheng, C. J.; Lo, M. F.; Xiao, J.; Lee, C. S.; Fung, M. K.; Zhang, X. H. A Multifunctional Phosphine Oxide-Diphenylamine Hybrid Compound as a High Performance Deep-Blue Fluorescent Emitter and Green Phosphorescent Host. *Chem. Commun.* **2014**, *50*, 2027−2029.
(28) Mallesham, G.; Swetha, C.; Niveditha, S.; Mohanty, M. E.; Babu, N. J.; Kumar, A.; Bhanuprakash, K.; Rao, V. J. Phosphine Oxide Functionalized Pyrenes as Efficient Blue Light Emitting Multifunctional Materials for Organic Light Emitting Diodes. *J. Mater. Chem. C* **2015**, *3*, 1208−1224.
(29) Møller, C.; Plesset, M. S. Note on an Approximation Treatment for Many-Electron Systems. *Phys. Rev.* **1934**, *46*, 618−622.
(30) Golebiew, A.; Parczews, A. Theoretical Conformational-Analysis of Organic-Molecules. *Chem. Rev.* **1974**, *74*, 519−530.
(31) Makino, S.; Kuntz, I. D. Automated Flexible Ligand Docking Method and Its Application for Database Search. *J. Comput. Chem.* **1997**, *18*, 1812−1825.
(32) Stahura, F. L.; Bajorath, J. New Methodologies for Ligand-Based Virtual Screening. *Curr. Pharm. Des.* **2005**, *11*, 1189−1202.
(33) Hay, B. P.; Oliferenko, A. A.; Uddin, J.; Zhang, C. G.; Firman, T. K. Search for Improved Host Architectures: Application of De Novo Structure-Based Design and High-Throughput Screening Methods to Identify Optimal Building Blocks for Multidentate Ethers. *J. Am. Chem. Soc.* **2005**, *127*, 17043−17053.
(34) Bryantsev, V. S.; Hay, B. P. De Novo Structure-Based Design of Bisurea Hosts for Tetrahedral Oxoanion Guests. *J. Am. Chem. Soc.* **2006**, *128*, 2035−2042.
(35) Allinger, N. L.; Yuh, Y. H.; Lii, J. H. Molecular Mechanics - the MM3 Force-Field for Hydrocarbons 0.1. *J. Am. Chem. Soc.* **1989**, *111*, 8551−8566.
(36) Gundertofte, K.; Liljefors, T.; Norrby, P. O. A Comparison of Conformational Energies Calculated by Several Molecular Mechanics Methods. *J. Comput. Chem.* **1996**, *17*, 429−449.
(37) Stewart, E. L.; Nevins, N.; Allinger, N. L.; Bowen, J. P. Molecular Mechanics (MM3) Calculations on Oxygen-Containing Phosphorus (Coordination IV) Compounds. *J. Org. Chem.* **1999**, *64*, 5350−5360.
(38) Stewart, E. L.; Nevins, N.; Allinger, N. L.; Bowen, J. P. Hartree-Fock and Moller-Plesset (MP2) Treatment of Oxygen-Containing Phosphorus Compounds. *J. Org. Chem.* **1997**, *62*, 5198−5207.
(39) Gordon, M. S.; Schmidt, M. W. Advances in Electronic Structure Theory: Gamess a Decade Later. In *Theory and Applications of Computational Chemistry: The First Forty Years*; Dykstra, C. E., Frenking, G., Kim, K. S., Scuseria, G. E., Eds.; Elsevier: Amsterdam, 2005.
(40) Schmidt, M. W.; Baldridge, K. K.; Boatz, J. A.; Elbert, S. T.; Gordon, M. S.; Jensen, J. H.; Koseki, S.; Matsunaga, N.; Nguyen, K. A.; Su, S. J.; Windus, T. L.; Dupuis, M.; Montgomery, J. A. General Atomic and Molecular Electronic-Structure System. *J. Comput. Chem.* **1993**, *14*, 1347−1363.
(41) Dunning, T. H. Gaussian-Basis Sets for Use in Correlated Molecular Calculations 0.1. The Atoms Boron through Neon and Hydrogen. *J. Chem. Phys.* **1989**, *90*, 1007−1023.
(42) Izgorodina, E. I.; Lin, C. Y.; Coote, M. L. Energy-Directed Tree Search: An Efficient Systematic Algorithm for Finding the Lowest Energy Conformation of Molecules. *Phys. Chem. Chem. Phys.* **2007**, *9*, 2507−2516.
(43) Xu, X.; Goddard, W. A. The Extended Perdew-Burke-Ernzerhof Functional with Improved Accuracy for Thermodynamic and Electronic Properties of Molecular Systems. *J. Chem. Phys.* **2004**, *121*, 4068−4082.
(44) Cambridge Structural Database, Version 5.35, Nov 2013.
(45) Allen, F. H. The Cambridge Structural Database: A Quarter of a Million Crystal Structures and Rising. *Acta Crystallogr., Sect. B: Struct. Sci.* **2002**, *58*, 380−388.
(46) Halgren, T. A. Merck Molecular Force Field 0.2. MMFF94 Van Der Waals and Electrostatic Parameters for Intermolecular Interactions. *J. Comput. Chem.* **1996**, *17*, 520−552.
(47) Halgren, T. A. Merck Molecular Force Field 0.5. Extension of MMFF94 Using Experimental Data, Additional Computational Data, and Empirical Rules. *J. Comput. Chem.* **1996**, *17*, 616−641.
(48) Halgren, T. A. Merck Molecular Force Field 0.3. Molecular Geometries and Vibrational Frequencies for MMFF94. *J. Comput. Chem.* **1996**, *17*, 553−586.
(49) Halgren, T. A. Merck Molecular Force Field 0.1. Basis, Form, Scope, Parameterization, and Performance of MMFF94. *J. Comput. Chem.* **1996**, *17*, 490−519.
(50) Halgren, T. A.; Nachbar, R. B. Merck Molecular Force Field 0.4. Conformational Energies and Geometries for MMFF94. *J. Comput. Chem.* **1996**, *17*, 587−615.
(51) Halgren, T. A. MMFF Vii. Characterization of MMFF94, MMFF94s, and Other Widely Available Force Fields for Conformational Energies and for Intermolecular-Interaction Energies and Geometries. *J. Comput. Chem.* **1999**, *20*, 730−748.
(52) Halgren, T. A. MMFF Vi. MMFF94s Option for Energy Minimization Studies. *J. Comput. Chem.* **1999**, *20*, 720−729.
(53) PCModel, Version 9.3, Serena Software: Bloomington, IN, 2011.
(54) Etter, M. C.; Baures, P. W. Triphenylphosphine Oxide as a Crystallization Aid. *J. Am. Chem. Soc.* **1988**, *110*, 639−640.

DOI: 10.1021/acs.jpca.5b04687
J. Phys. Chem. A 2015, 119, 8765−8773